Prediction of Iron Ore Grade using Artificial Neural Network, Computational Method, and Geo-statistical Technique at El-Gezera Area, Western Desert, Egypt

Ashraf F. Ismael[1,2], Abdelrahem Embaby[*1], Faisal A. Ali[1], H. A. Farag[1], Sayed Gomaa[1], Mohamed Elwageeh[3], and B.G. Mousa[1]

1. Department of Mining and Petroleum Engineering, Faculty of Engineering, Al-Azhar University, Cairo, Egypt
2. Faculty of Engineering and Technology, Future University in Egypt (FUE), Cairo, Egypt
3. Mining, Petroleum, and Metallurgical Engineering Department, Faculty of Engineering, Cairo University, Cairo, Egypt

Article Info	Abstract
	The mineral resource estimation process necessitates a precise prediction of the grade based on limited drilling data. Grade is crucial factor in the selection of various mining projects for investment and development. When stationary requirements are not met, geo-statistical approaches for reserve estimation are challenging to apply. Artificial Neural Networks (ANNs) are a better alternative to geo-statistical techniques since they take less processing time to create and apply. For forecasting the iron ore grade at El-Gezera region in El- Baharya Oasis, Western Desert of Egypt, a novel Artificial Neural Network (ANN) model, geo-statistical methods (Variograms and Ordinary kriging), and Triangulation Irregular Network (TIN) were employed in this study. The geo-statistical models and TIN technique revealed a distinct distribution of iron ore elements in the studied area. Initially, the tan sigmoid and logistic sigmoid functions at various numbers of neurons were compared to choose the best ANN model of one and two hidden layers using the Levenberg-Marquardt pure-linear output function. The presented ANN model estimates the iron ore as a function of the grades of Cl%, SiO2%, and MnO% with a correlation factor of 0.94. The proposed ANN model can be applied to any other dataset within the range with acceptable accuracy.

1. Introduction

One of the most crucial concepts and difficult mining process phases is mineral resource estimation. It is important in the decision-making process for mining investments including pit design, production scheduling, and grade control, as previously covered [1-9].

The main purpose of mineral resource estimation is to determine the mineral grade at a location with limited drilling data [10]. Owing to complicated geological activity of an era, the spatial distribution of mineral deposits is unpredictable. Thus estimating mineral resources at an unsampled site is difficult [11, 12].

Artificial Neural Networks (ANNs) are effective computer-based substitutes for calculating mineral reserves [1]. A computer model

called a neural network is based on the structure of neuron cells in the biological nervous system. The neural network may learn the data pattern with the help of a learning algorithm and a training batch of data [13–15]. When the second-order stationary assumption regarding the spatial distribution of ore grade inside the ore body is not met, the learning ability of ANNs offers an exciting alternative to conventional geostatistical ore reserve calculation [1, 16, 17]. Additionally, the grade of spatial variability is captured by ANNs using a nonlinear input-output mapping via a set of connection weights (global fitting model), as opposed to Kriging, which uses nearby sample points to estimate the grade of a specific place using a linear weighting (local fitting model). Yet there is no

✉ *Corresponding author: Abdel-raheemkhalifa.12@azhar.edu.eg (A. Embaby).*

requirement for experimental variogram calculations in the ANNs method with a small amount of input data [18]. Because geostatistical calculations require a certain number of samples, the calculation of variograms becomes progressively uncertain, if not impossible [19, 20]. Geostatistical calculations also necessitate the use of appropriate computer systems and a rigorous mathematical foundation [21, 22].

Artificial neural networks have proven to be a reliable and fast method in a variety of sectors, turning out to be a good selection when you need a comprehensive predictive analysis with many variables [23]. Neural networks are capable of capturing erratic and extremely complicated interactions between process inputs and outputs. They are effective in terms of computing and do not require prior knowledge of the depicted process [24].

A few data points presented as sampling with known locations in 3D space are utilized as input data for grade estimation using neural networks, and the grade attribute is an output for the relevant datasets. A network captures the complex spatial organization of input and output patterns using a collection of link weights that are modified during network training. Through training, the network captures an input-output relationship and gains some prediction power, allowing it to provide output (grades) for a certain input (northing, easting, and elevation coordinates). The hidden and output layers of a neural network can employ various activation functions.

This research work aims to suggest ANN-based models to calculate the grade of iron ore as a function of Cl%, SiO_2%, and MnO% in El-Gezera area in the Bahariya oasis, Egypt. In addition, GIS and geo-statistical-based modeling is introduced to anticipate the spatial distribution of Fe%, MnO%, Cl%, and SiO_2% and create distribution maps for various items based on grades. The whole work is done in 2D based on composite samples.

2. Description of El-Gezera Area

The Bahariya oasis area and the area around the Bahariya Depression, where hematite and limonite are visible on the surface, are rich in iron ore resources [25, 26]. The iron ores are located in the main four areas within Bahariya Oasis, which include El-Gedida, El-Haraa, Ghorabi, and Naser mines. El-Gezera area is bounded by latitudes 28° 26' 10.5″ and 28° 25' 44.5″ N and longitudes 29° 10' 21.5″ and 29° 11' 27.5″ E. El-Gezera area is a new extension for El-Gedida iron ore mine, as shown in

Figure 1. El-Gedida region is situated on El-Bahariya depression's northeastern plateau. Latitude 28° 27' N and longitude 29° 10' are the approximate coordinates of El-Gedida area's core. El-Gedida iron ore deposit is part of Bahariya Oasis and it is the largest and richest iron ore deposit in Egypt's Western Desert [27]. In this study, the dataset (Fe%, MnO%, Cl%, and SiO_2%) was collected from 74 drill holes distributed over the study area as shown in Figure 2. These datasets include coordinates (north and east), altitudes, ore thickness, and chemical analyses of the samples retrieved from boreholes.

3. Geologic Setting of El-Gezera Area

El-Gezera and El-Gedida mines are near the northeastern coast plateau of the Bahariya Oasis depression in Egypt's Western Desert, which is an oval-shaped depression surrounded by deteriorated karst cone hills from the Naqb Formation. A high relief characterizes the central part of the depression, which is peppered by prominent hills. Lyon's hill, at 254.5 meters above sea level and 42 meters over the plateau surface of the high center area, is the highest hill. The Naqb Formation's highly silicified nummulitic limestone makes up these hills. Passing through a hard silcrete crust on the northern half of the depression's floor. The low wadi region, which rises to 198 meters above sea level, surrounds the high mountain core area and its related relict hills. On the northern part of the depression's floor, there are some silcrete hillocks. The high center area and wadi area, except for the prominent hills, are mostly iron ore deposits that lie unconformably underlying the Bahariya formation. A major anticline and normal, significant faults are the main structural components of El-Gezera interior and the El-Gedida mine area. The Bahariya Formation has an impact on the anticline. It strikes NE-SW and plunges to the northeast. The faults have NE-SW, N-S, and NW-SE trends. The tectonic phase that predominated towards the end of the Oligocene and activated ancient structures may be connected to these significant faults [28, 29]. The geologic setting of El-Gedida mine area and El-Gezera area is shown in Figure 3.

In local areas, upon the submarine swells of the northeastern plateau of the Bahariy Depression (e.g. El Gedida, El Gezera, El Harra, and Ghorabi mine areas), the Lutetian carbonate sequence changes entirely into a condensed section of oncolitic-oolitic and nummulitic ironstone facies (iron ores) punctuated by several deposition breaks and unconformities. The ore stratigraphic profile

represents an unconformity-bounded reduced section underlain by the Cenomanian clastics and overlain by the Lutetian-Bartonian glauconitic sequence and/or Oligocene fluvial sediments [30].
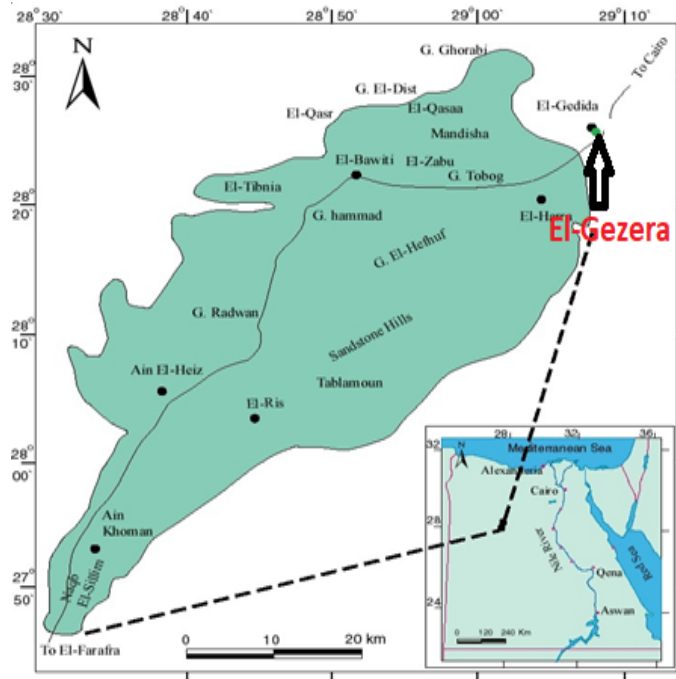

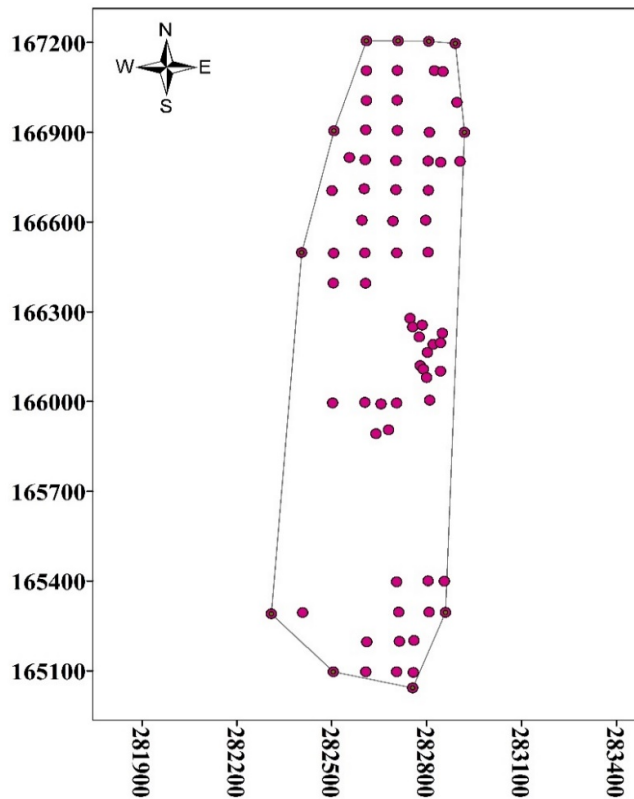**Figure 1. Location map of El-Gezera iron ore area.**

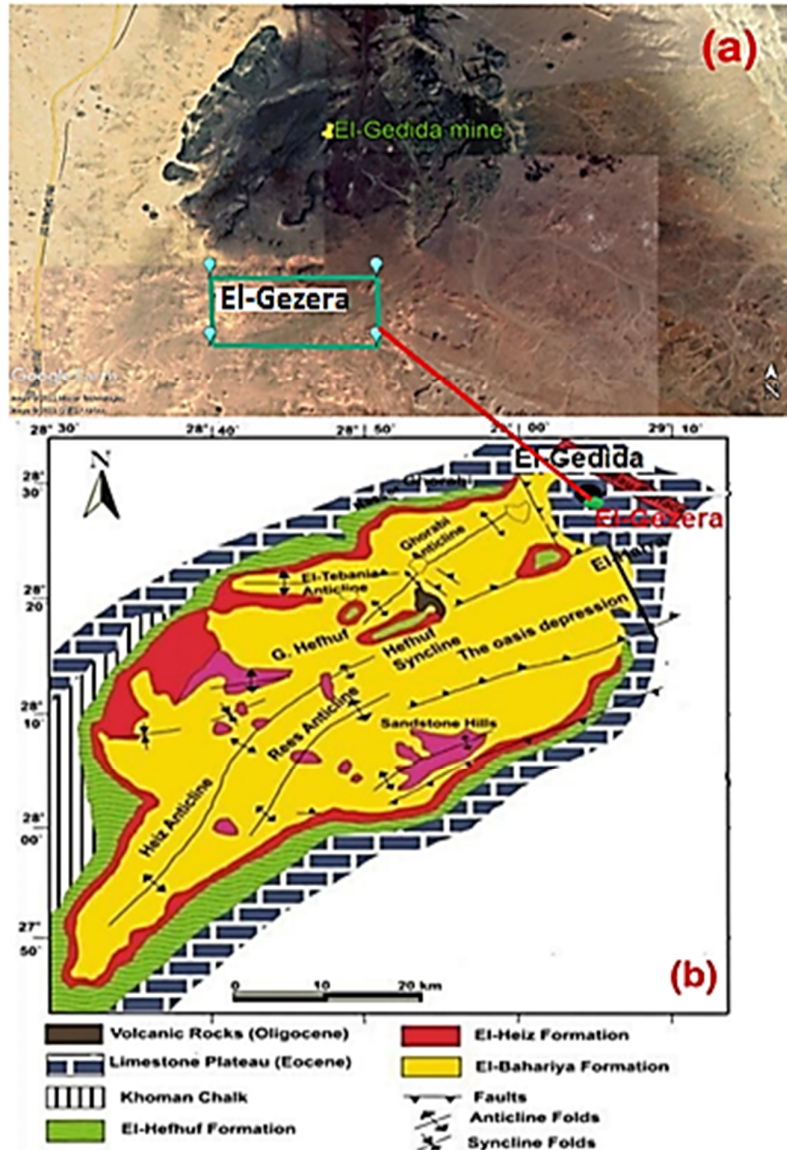**Figure 2. Boreholes distribution over the studied area.**

Figure 3. a) Google Earth picture of El-Gezera region, b) Bahariya Oasis geological map, western desert, Egypt showing El-Gezera mine area [28–31].

4. Methods
4.1. GIS analysis

A triangulated irregular network (TIN) was employed in this study to examine the spatial distribution of iron ore elements. A surface is represented by the TIN as a collection of irregularly spaced points connected by lines, creating a network of neighboring triangles that don't overlap of various sizes and proportions. The x, y, and z values are stored in each triangle node [32]. When it comes to surface analysis, TINs have a lot of benefits. First, they include the original sample points, which serve as a useful check on the model's accuracy. Secondly, because of the variable density of triangles, a TIN is an effective way to store

surface characterizations such as terrains with significant topographic variations. Finally, the data structure makes calculating elevation, aspect, slope, and line-of-sight between points a breeze. The TIN data structure has become widely used in applications such as volumetric computation for roadway design, drainage research for land development, and visualization of urban forms due to a combination of these variables [33-35].

4.2. Variogram and Kriged models

The variogram is a graph that displays the spatial variability of $x(u_a)$, where u_a is the coordinate vector at each of the observation points $a = (1, 2, 3, ... N)$ for the variable x. The average

quadratic difference between two observations of a variable separated by a distance-vector h is half what is known as the empirical variogram $\gamma(h)$ [36, 37]:

$$\gamma(h) = \frac{1}{2N(h)} \sum_{a=1}^{N(h)} [x(u_a) - x(u_a + h)]^2 \quad (1)$$

The experimental variogram was fitted with the three most widely used theoretical variogram models, as measured below [36]:

Spherical model:

$$\begin{cases} \gamma(h) = C_0 + \left[\frac{3h}{2a} - \frac{1}{2}\left[\frac{h}{a}\right]^3\right] \\ \gamma(h) = C \end{cases} \begin{matrix} for\, h < a \\ for\, h \geq a \end{matrix} \quad (2)$$

Experimental model:

$$\gamma(h) = C_0 + \left\{1 - exp\left(\frac{-3h}{a}\right)\right\} \quad (3)$$

Gaussian model:

$$\gamma(h) = C_0 + \left\{1 - exp\left(\frac{-3h^2}{a^2}\right)\right\} \quad (4)$$

Kriging is a method for getting the best, most objective estimates of regionalized variables in unsampled areas by utilizing the structural properties of the variogram and the initial set of data values. Since Kriging takes the spatial structure of the parameter into account, it performs better than other methods including the arithmetic mean technique, the closest neighbour method, the distance weighted method, and polynomial interpolation. The estimation variance at each estimated point is also provided via kriging, which is a measure of the estimated value's accuracy. This is seen as kriging's primary benefit over other estimating methods [37].

The mean can vary spatially using ordinary kriging (OK): the mean is estimated for each prediction neighborhood. The weighted averages of the available data are used to make OK predictions. The best linear unbiased predictor is defined by the OK weights (BLUP). The OK

forecasting, $Z(x_0)_{ok}$, is defined as [38], [39], and [40]:

$$Z(x_0)_{ok} = \sum_{n=1}^{n} \lambda_a^{ok} Z(x_a) \quad (5)$$

Given the requirement that the weights, λ_a^{ok} OK, equal to 1, in order to provide an unbiased prediction:

$$\sum_{n=1}^{n} \lambda_a^{ok} = 1 \quad (6)$$

As a result, the kriging system aims to discover suitable weights to multiply the given observations before summing them to get the anticipated value. The model's coefficients fitted to the variogram are used to calculate these weights (or a different function like the covariance function). The forecasted value of the kriging prediction error must be zero:

$$E\{Z(x_0)_{ok} - Z(x_0)\} = 0 \quad (7)$$

The kriging (or prediction) variance is written as $\sigma_{ok}^2(x_0)$:

$$\sigma_{ok}^2(x_0) = E[\{Z(x_0)_{ok} - Z(x_0)\}^2]$$

$$\gamma(0) - \sum_{a=1}^{n}\sum_{\beta=1}^{n} \lambda_a^{ok}\lambda_\beta^{ok}\gamma(x_a - x_\beta) +$$

$$2\sum_{a=1}^{n} \lambda_a^{ok}\gamma(x_a - x_0) \quad (8)$$

Thus we look for the values of $\lambda_1 \dots \dots \dots \dots \dots \lambda_n$ (the weights) that minimal this expression with the constraint that the weights sum equal to one (Eq. (6)). Lagrange multipliers are used to achieve this minimization. The OK system, which consists of n + 1 equation and n + 1 unknown, specifies the minimization requirements:

$$\sum_{\beta=1}^{n} \lambda_\beta^{ok}\gamma(x_a - x_\beta) + \psi_{ak} = \gamma(x_a - x_\beta)a = 1, \dots, n$$

$$\sum_{\beta=1}^{n} \lambda_\beta^{ok} = 1 \quad (9)$$

where ψ_{ok} is a Lagrange muliplier. Knowing ψ_{ok}, the OK's prediction variance may be expressed as:

$$\sigma_{ok}^2 = \psi_{ok} - \gamma(0) + \sum_{a=1}^{n} \lambda_a^{ok} \gamma(x_a - x_0) \quad (10)$$

4.3. Artificial neural networks model

In this study, an ANN model was developed using MATLAB software to predict the ore grade as a function of Cl%, SiO$_2$%, and MnO%. The developed model was trained validated and tested using 70% (52 datasets), 15% (11), and 15% (11 datasets). The correlation between the input parameters and the output parameters is first checked as shown in **Figure 4**. After that all the datasets are normalized, and transformed and then we check various models at different numbers of neurons for the hidden layer. The optimization technique used in this study is Levenberg-Marquardt technique. Levenberg-Marquardt technique is one of the built-in MATLAB software techniques. This is trial and error technique used to compare between the model predicted values and the actual values. This technique is used to solve nonlinear least squares problems by minimizing the sum of the squares of the errors between the model predicted values and the actual ones. The Levenberg-Marquardt algorithm combines two numerical minimization algorithms: the gradient descent method and the Gauss-Newton method. In the gradient descent method, the sum of the squared errors is reduced by updating the parameters in the steepest-descent direction. In the Gauss-Newton method, the sum of the squared errors is reduced by assuming the least square's function is locally quadratic in the parameters and finding the minimum of this quadratic. The developed model is described in Section 5.4.

5 . Results and discussion
5.1. Statistical analysis

Statistical analysis is a tool that assists in drawing useful inferences from raw and unstructured information [41], [42], [43], [44], and [45]. The statistical analysis as presented in Table 1 shows the statistical description of the data, where Cl% ranges from 0.26 to 3.41, SiO$_2$% ranges from 3.67 to 21.17, MnO% ranges from 0.02 to 3.08, and iron ore grade ranges from 40.76 to 59.1. Figure 4 indicates that the iron ore grade is directly proportional to MnO% and Cl% and inversely proportional to SiO$_2$%.

Table 1. Statistical analysis of the iron ore elements.

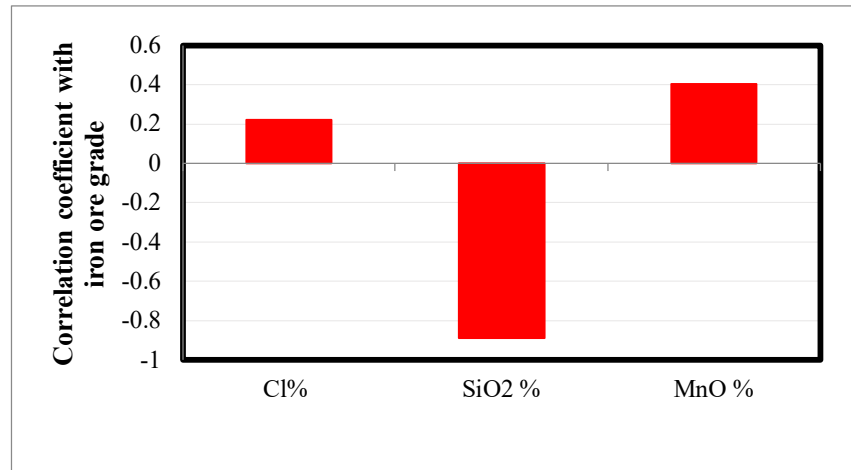| Statistical parameters	Cl, %	SiO$_2$, %	MnO, %	Fe, %
Minimum	0.26	3.67	0.02	40.76
Maximum	3.41	21.17	3.08	59.10
Mean	0.93	10.04	0.48	50.9
Stan. error	0.06	0.50	0.06	0.50
Variance	0.29	18.00	0.26	17.68
Stan. deviation	0.54	4.24	0.51	4.20
Range	3.15	17.5	3.06	18.34
Co. of variation	0.58	0.42	1.06	0.08
Kurtosis	7.06	2.58	11.25	2.05
Skewness	1.57	0.58	2.45	-0.18

Figure 4. Correlation coefficients between iron ore grade and input parameters.

5.2. Spatial distribution of iron ore elements

The interpolated TIN was used to construct iso-chemical maps for iron ore elements distributions in El-Gezera iron ore mine, as shown in Figure 5. This TIN was classified, where each class has a specific color and represents a specific percentage of iron ore element. The Fe percentages in the El-Gezera iron ore mine range from 40.76 to 59.1, while the average Fe percentage in the whole mine is 50.87. The regions with the highest Fe% are distributed in the east part of the mine, while the regions with the lowest Fe% are concentrated in the center part of the mine toward the south. Also, the results showed that the Fe% distribution decreased in the direction from east to west. The Cl percentages in the El-Gezera iron ore mine range from 0.26 to 3.41, while the overall average of Cl% in the mine is 0.94. The Cl% distribution increases in the direction from west to east, while the region with the highest Cl% is concentrated in the upper east of the El-Gezera mine. The SiO_2% in El-Gezera mine ranges from 3.67 to 21.17, while the average SiO_2% in the whole mine is 10.05. The SiO_2% distribution increases from east to west, while the regions with the highest SiO_2% are concentrated in the extension between the center and west of the El-Gezera mine. The MnO percentages range from 0.02 to 3.08, while the average MnO% in the whole mine is 0.49. The MnO% distribution increases from west to east, while the regions with the highest MnO% are concentrated in the east part of El-Gezera area. The majority of MnO% in El-Gezera mine is less than 0.4%, which is distributed in the west part of the mine.
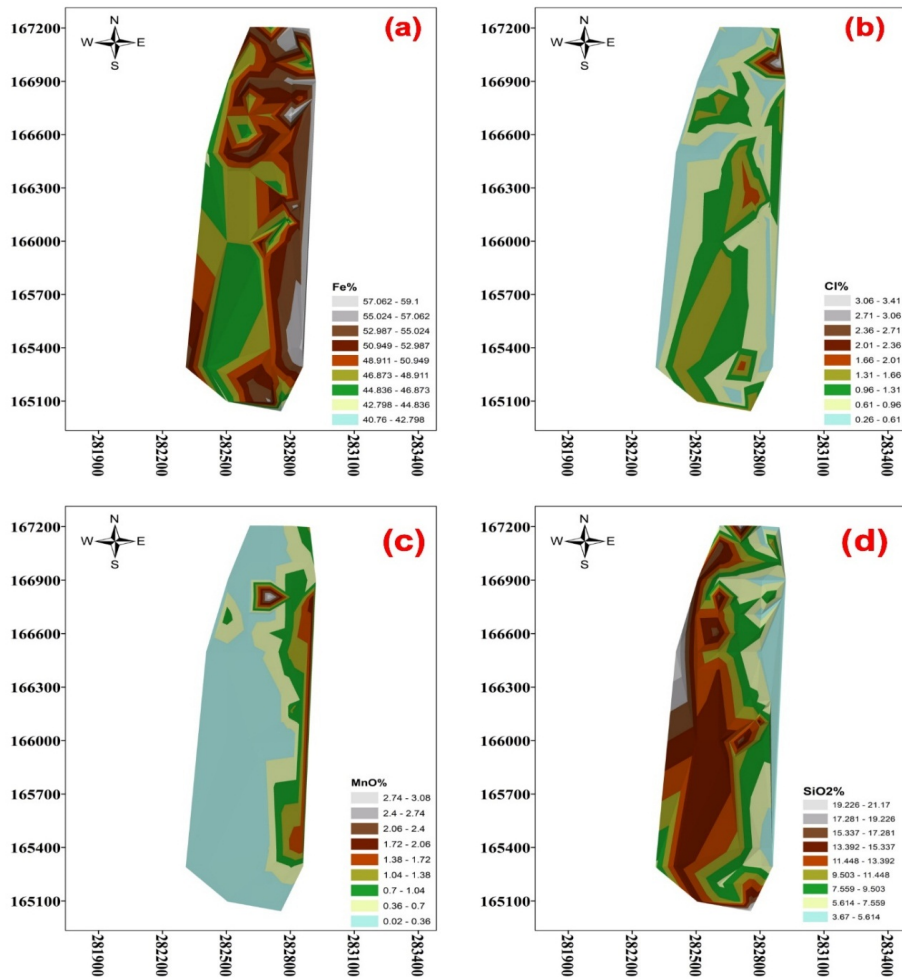
Figure 5. Iso-chemical maps of iron ore elements distribution in the El-Gezera iron ore mine: (a) Fe% distribution, (b) Cl% distribution, (c) MnO% distribution, and (d) SiO₂% distribution.

5.3. Geostatistical analysis
5.3.1. Construction of variograms

The construction of a variogram is the first step in any geo-statistical study, and has a vital role in the ore evaluation process. The selected variogram model will be used in the kriging calculation and will affect all results and conclusions. A global variogram was constructed using GS$^+$ program for Cl%, SiO₂%, MnO, and Fe% depending on the available data for each parameter, and a spherical model was selected as a more suitable model for Cl%, SiO₂%, and Fe%, whereas a Gaussian model was selected for MnO%, as shown in Figure 6. The variogram parameters for Cl%, SiO₂%, MnO%, and Fe% in the studied area are summarized in Table 2.
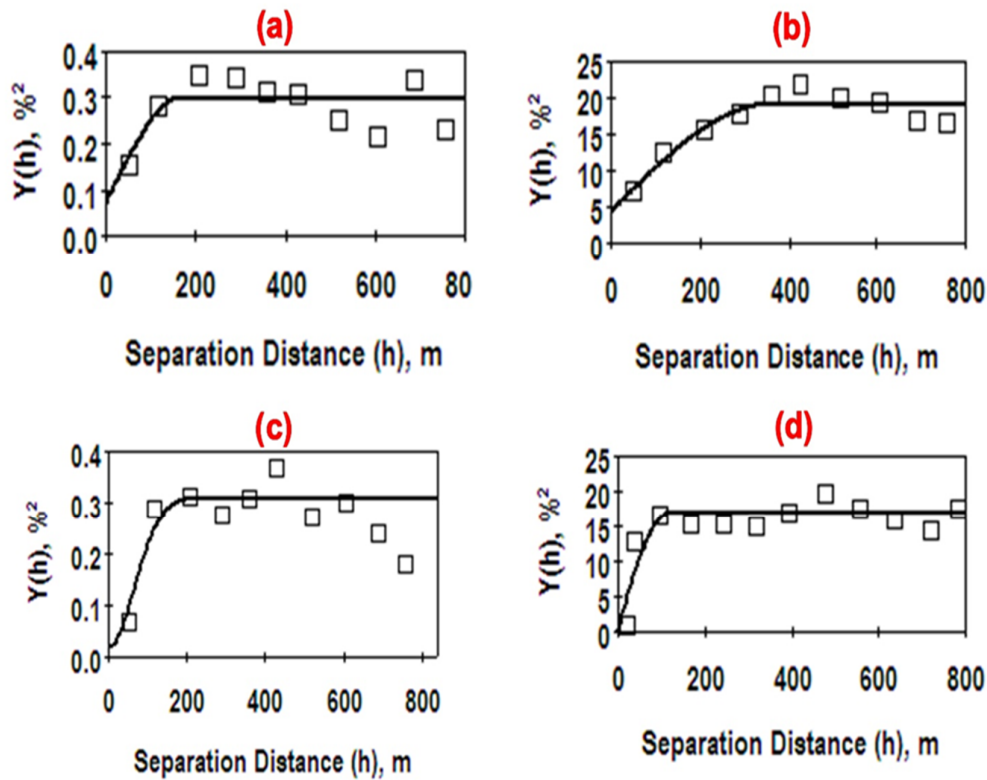
Figure 6. Variogram models for iron ore elements at the El-Gezera area: (a) Spherical variogram model for Cl%, (b) Spherical variogram model for SiO₂%, (c) Gaussian variogram model for MnO%, (d) Spherical variogram model for Fe %.

Table 2. Variogram parameters of the iron ore dataset.

Variogram parameters	Cl%	SiO₂%	MnO%	Fe%
Type	Spherical	Spherical	Gaussian	Spherical
Direction	Global	Global	Global	Global
Range, m	167	356	162	114
Nugget effect (C0), %2	0.07	4	0.02	0
Sill (C), %2	0.3	19	0.31	16.8
Screen effect ratio C0/C	0.23	0.21	0.06	0

5.3.2. Kriged models

Ordinary Kriging was used to interpolate unsampled locations by creating map analyses that show the spatial distribution of Cl%, SiO₂%, MnO%, and Fe% in the studied area, as shown in Figure 7, depending on the selected variogram model for each one. Maps are classified into colures; each color represents a definite range of percentages of Cl%, SiO₂%, MnO%, and Fe%. As shown in Figure 7, the low percent of Cl is located in the NW direction of the studied area; on the other hand, the lowest percentages of SiO₂ are located in

the NE direction. Also both MnO and Fe have the highest percentages in the NE direction. The rest of the studied area is characterized by high percentages of Cl and SiO₂, which require more attention in the production stage to adjust to an allowable percent, which is preferable in iron production by blast furnace technique. Also maps indicate that most of the Fe% and MnO% are suitable for the iron production processes, except for small pockets that need little attention in the production stage. In general, the iron ore and its impurities in the studied area are suitable for steel production by blast furnace technique.
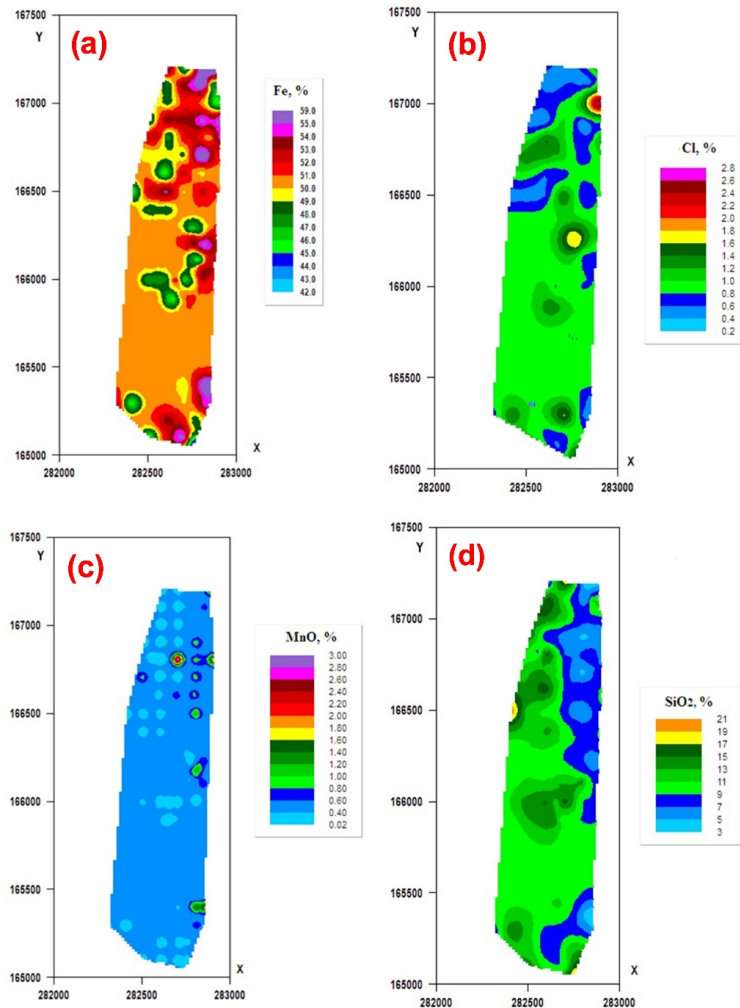
Figure 7. Kriged models of iron ore elements at the El-Gezera iron ore mine: (a) Fe% distribution, (b) Cl% distribution, (c) MnO% distribution, and (d) SiO₂% distribution.

5.4. ANN model optimization and description

The proposed model is composed of three layers. The input layer, for example, contains three neurons for the input parameters of Cl%, SiO$_2$%, and MnO%. There are 12 neural cells in the hidden layer. One neuron is included for the output layer's output parameter, which is the iron ore grade. To find the best ANN model, we compared the tan sigmoid *vs.* logistic sigmoid functions for one hidden layer at different numbers of hidden neurons (6, 7, 8, 9, 10, 11, and 12), as shown in Tables 3 and 4. Then for two hidden layers, we

compared the tan sigmoid as a transfer function to the logistic sigmoid functions at varied numbers of hidden neurons (10, 11, and 12).

The logistic sigmoid function with one hidden layer of 12 neurons was discovered to be the most optimal case. The model with these properties has the highest correlation coefficient (0.94) as well as the lowest RMSE (1.47%). We arrived at this conclusion using the Levenberg-Marquardt optimization technique and an output function that is pure linear. Table 6 lists the proposed model's properties, while Figures 8 and 9 depict the suggested ANN architecture.

Table 3. Tan sigmoid function accuracy evaluation at various neuronal densities for a single hidden layer.

Parameters	6	7	8	9	10	11	12
R	0.895	0.935	0.921	0.898	0.811	0.941	0.926
SD	4.43	3.26	3.4	3.96	5.801	3.061	3.579
RMSE	2.042	1.641	1.673	2.013	2.808	1.516	1.823
MRE	0.446	0.046	0.208	-0.316	1.573	-0.363	-0.513
MAE	3.289	2.529	2.592	2.876	3.973	2.158	2.597

Table 4. Sigmoid function accuracy evaluation at various neuron counts for a single hidden layer.

Parameters	6	7	8	9	10	11	12
R	0.908	0.934	0.829	0.932	0.915	0.914	0.94
SD	3.654	3.443	4.547	3.334	4.142	3.448	2.951
RMSE	1.83	1.656	2.307	1.704	1.957	1.71	1.478
RE	0.165	-0.697	2.148	1.495	0.193	-0.18	0.098
AE	2.887	2.686	3.671	2.65	3.094	2.666	2.132

Table 5. Evaluation of accuracy for two hidden layers using sigmoid and tan sigmoid functions for various numbers of neurons.

Parameters	1010T	1010S	1111T	1111S	1212T	1212S
R	0.901	0.931	0.941	0.914	0.918	0.933
SD	4.427	3.449	3.061	3.448	3.592	3.392
RMSE	2.107	1.695	1.516	1.71	1.742	1.68
RE	-1.527	-0.388	-0.363	-0.18	-0.672	0.045
AE	3.356	2.649	2.158	2.666	2.718	2.519

Table 6. lists the attributes of the suggested ANN model.

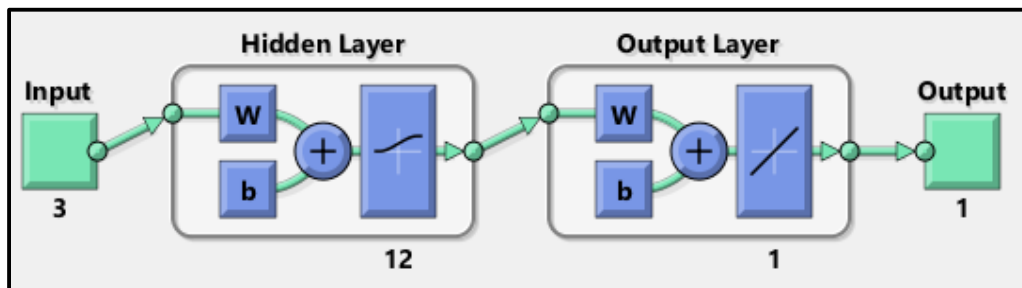| Parameter	Value
No. of layers	Three
Number of neurons in the input layer	Three
Count of neurons in the hidden layer	twelve
Training algorithm	Levenberg-Marquardt
The algorithm layer's activation process	Logistic sigmoid
The output layer's ability to activate	Pure-linear

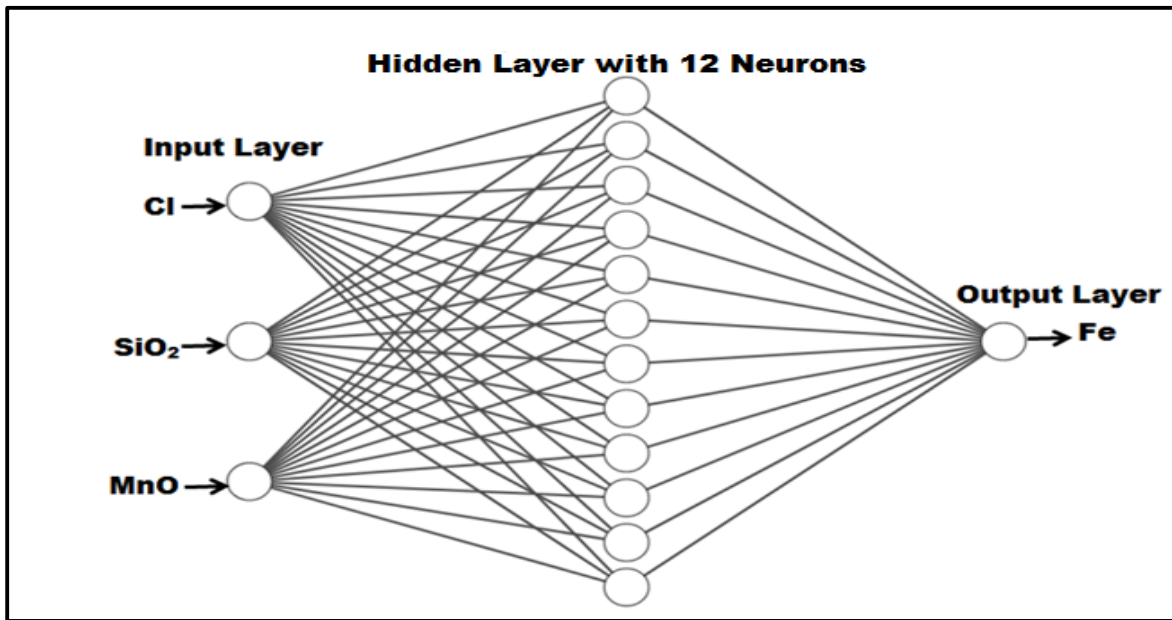**Figure 8. The suggested ANN model for estimating iron content.**

Figure 9. Depicts the architectural design of the proposed ANN model for iron content estimation.

The following equations are used to normalize the real input parameters for each dataset:

$$Cl_n = 0.634921Cl - 1.165079 \qquad (11)$$

$$SiO2_n = 0.067204SiO2 - 1.24664 \qquad (12)$$

$$MnO_n = 0.653595MnO - 1.013072 \qquad (13)$$

The iron ore grade (IOG), which is stated in Eq. 14, is calculated using the normalized parameters for each dataset and the model coefficients for each neuron in Table 7.

$$IOG = 13.185 \left[\sum \left(\frac{w_{hi}}{1 + e^{-[Cl_n W_{i,1} + SiO2_n W_{i,2} + MnO W_{i,3} + b_i]}} \right) + b_{hi} \right] + 45.915 \qquad (14)$$

where b_i represents the bias of neuron i, b_{hi} is the bias of hidden layer, and $W_{i,1}, W_{i,2}, W_{i,3}$ represent the weight of neuron i and inputs 1, 2, and 3, respectively. w_{hi} represent the weight of the hidden neuron i.

Table 7. Coefficients of the proposed model.

i	$W_{i,1}$	$W_{i,2}$	$W_{i,3}$	b_i	W_{hi}	b_{hi}
1	6.9216	1.3239	-0.46593	-5.8893	-1.6456	0.48331
2	-5.2527	0.44629	3.556	5.5244	-0.85084	
3	4.9567	3.7406	1.4072	-4.0856	0.41816	
4	5.9483	2.5124	1.8044	-2.9855	-1.0177	
5	3.0611	4.2142	3.7521	-1.7646	0.012133	
6	-3.0765	6.0548	6.1678	4.7859	-0.58613	
7	-4.739	-5.0098	-1.9871	-5.1214	0.412	
8	-3.8942	-2.7984	-9.4329	-7.5697	-0.75808	
9	2.1839	-4.554	-3.9374	3.0022	1.0912	
10	-3.22	-3.6835	5.0078	-2.4559	0.4085	
11	1.8354	1.6825	-5.9187	6.1958	-0.11845	
12	-5.381	-2.5286	-5.991	-9.1067	0.37113	

The proposed ANN model's iron ore grade predictions are shown against the actual values for training, validation, and all data sets in Figures 10,11, and 12. The data points are close to the unit-slope line, which shows how accurate the model is; for the training, validation, and all datasets, the correlation coefficients are 0.93, 0.991, and 0.943, respectively.
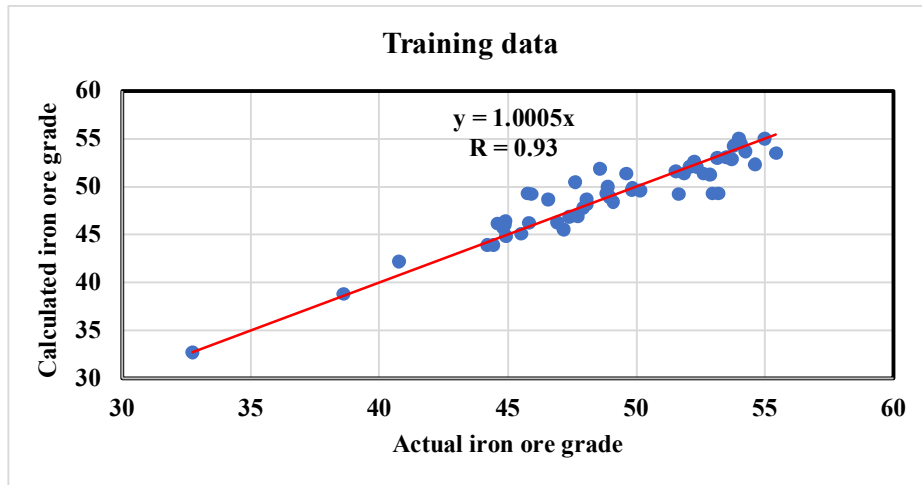
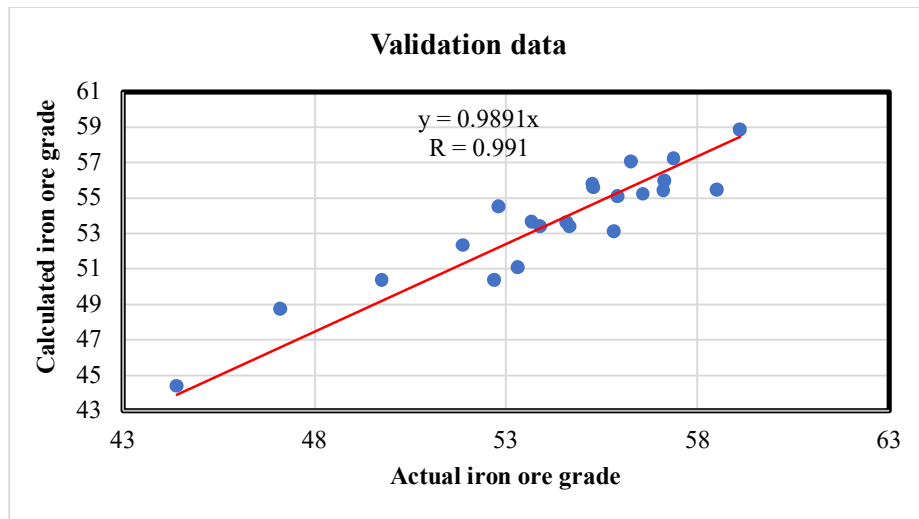**Figure 10. Cross-plot of training data; the suggested model.**

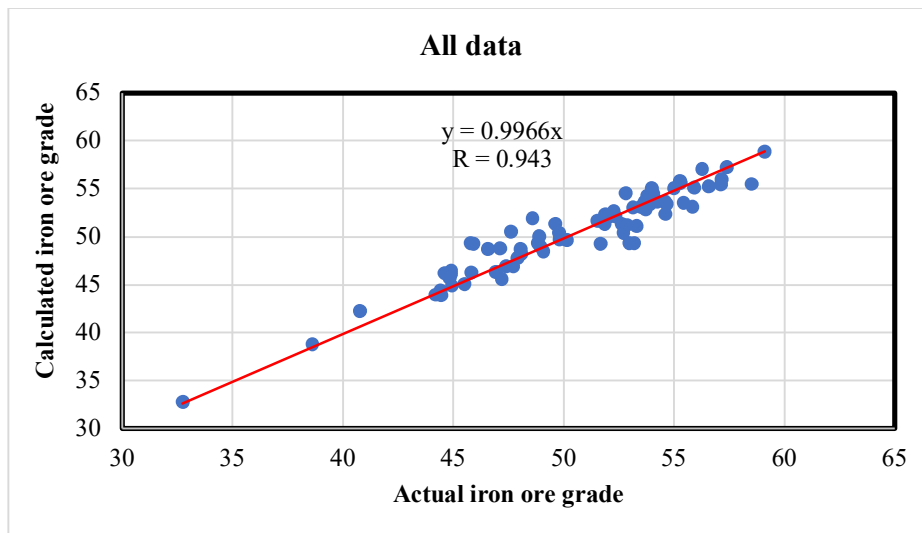**Figure 11. Cross plot of validation data of the suggested model.**

Figure 12. Cross-plot of all the data from the suggested model.

6. Conclusions

In this paper, the iron ore grade (Fe%, MnO%, Cl%, and SiO$_2$%) in the El-Gezera area has been predicted using Triangulation Irregular Network (TIN) methods, geostatistical-based modeling, and Artificial Neural Network (ANN) model. The following conclusions can be drawn:

The TIN method for iron ore elements distributions proved that the regions with the highest Fe% are distributed in the east part of the mine, while the regions with the lowest Fe% are concentrated in the center part of the mine toward the south. Also, the Fe% distribution decreases from east to west. The Cl% distribution increases from west to east, while the region with the highest Cl% is concentrated in the upper east of El-Gezera mine. The SiO$_2$ % distribution increases from east to west, while the regions with the highest SiO$_2$% are concentrated in the extension between the center and west of El-Gezera mine. The MnO% distribution increases from west to east, while the regions with the highest MnO% are concentrated in the east part of El-Gezera area. The majority of MnO% in El-Gezera mine is less than 0.4%, which is distributed in the west part of the mine.

The constructed variograms kriged models for iron ore elements in El-Gezera area showed that the lowest percentage of Cl is located in the NW direction of the studied area; on the other hand, the lowest percentages of SiO$_2$ are located in the NE direction. Also, both MnO and Fe high percent are located in the NE direction. The rest of the studied area suffered from high percentages of Cl and SiO$_2$.

With a correlation coefficient of 0.94, a novel artificial neural network (ANN)-based empirical correlation was created for calculating the iron grade as a function of MnO%, Cl%, and SiO$_2$%. Without having to write any code, the suggested ANN model may be used to predict the iron grade for other datasets that fall within the range.

Furthermore, most of the Fe% and MnO% are suitable for the iron production processes, except for small pockets that need little attention in the production stage. In general, the iron ore with its impurities in the studied area are still suitable for steel production by blast furnace technique.

References

[1]. Dumakor-Dupey, N. K., & Arya, S. (2021). Machine learning—a review of applications in mineral resource estimation. *Energies, 14*(14), 4079.

[2]. Galetakis, M., Vasileiou, A., Rogdaki, A., Deligiorgis, V., & Raka, S. (2022). Estimation of mineral resources with machine learning techniques. Materials Proceedings, 5(1), 122.

[3]. Tariq, A., Yan, J., Ghaffar, B., Qin, S., Mousa, B. G., Sharifi, A., ... & Aslam, M. (2022). Flash flood susceptibility assessment and zonation by integrating analytic hierarchy process and frequency ratio model with diverse spatial data. Water, 14(19), 3069.

[4]. Jinchuan, Ke. (2002). Neural-network modelling of placer ore grade spatial variability. Dissertation, University of Alaska, Fairbanks.

[5]. Yasrebi, A. B., Hezarkhani, A., Afzal, P., Karami, R., Tehrani, M. E., & Borumandnia, A. (2020). Application of an ordinary kriging–artificial neural network for elemental distribution in Kahang porphyry deposit, Central Iran. *Arabian Journal of Geosciences*, *13*(15).

[6]. Mahmoudabadi, H., Mohammad, I., & Mohammad, B.M. (2009) A hybrid method for grade estimation using genetic algorithm and neural networks. *Comput Geosci*, *13*:91–101.

[7]. Chiroma, H., Noor, A. S. M., Abdulkareem, S., Abubakar, A. I., Hermawan, A., Qin, H., ... & Herawan, T. (2017). Neural networks optimization through genetic algorithm searches: a review. *Appl. Math. Inf. Sci*, *11*(6), 1543-1564.

[8]. Tahmasebi, P., & Hezarkhani, A., (2010). Comparison of optimized neural network with fuzzy logic for ore grade estimation. *Aust J Basic Appl Sci*, *4*(5):764–772.

[9]. Tahmasebi, P., & Hezarkhani, A. (2012). A hybrid neural networks-fuzzy logic- genetic algorithm for grade estimation. *Comput Geosci*, *42*, 18–27.

[10]. Li, XL., Li, LH., Zhang, BL., & Guo, QJ. (2013). Hybrid self-adaptive learning based particle swarm optimization and support vector regression model for grade estimation. *Neurocomputi*ng *118.* 179–190.

[11] Dutta, S., Bandopadhyay, S., Ganguli, R., & Misra, D. (2010). Machine learning algorithms and their application to ore reserve estimation of sparse and imprecise data. *Journal of Intelligent Learning Systems and Applications*, *2*(02), 86-96.

[12]. Embaby, A., Ismael, A., Ali, F. A., Farag, H. A., Mousa, B. G., Gomaa, S., & Elwageeh, M. (2023). An approach based on Machine Learning Algorithms, Geostatistical Technique, and GIS analysis to estimate phosphate ore grade at the Abu Tartur Mine, Western Desert, Egypt. *Min. Depos, 17*(1).

[13]. Afzal, P., Farhadi, S., Konari, M. B., Meigoony, M. S., & Saein, L. D. (2022). Geochemical Anomaly Detection in the Irankuh District Using Hybrid Machine Learning Technique and Fractal Modeling. *Geopersia*, *12*(1), 191–199.

[14]. Farhadi, S., Afzal, P., Konari, M. B., Saein, L. D., & Sadeghi, B. (2022). Combination of Machine

Learning Algorithms with Concentration-Area Fractal Method for Soil Geochemical Anomaly Detection in Sediment-Hosted Irankuh Pb-Zn Deposit, Central Iran. *Minerals 2022, Vol. 12, Page 689*, *12*(6), 689.

[15]. Mostafaei, Kamran., & Ramazi, H. (2019a). Investigating the applicability of induced polarization method in ore modelling and drilling optimization: a case study from Abassabad, Iran. *Near Surface Geophysics*, *17*(6), 637–652.

[16]. Waqas, H., Shang, J., Munir, I., Ullah, S.; Khan, R., Tayyab, M., Mousa, B.G., Williams, S. (2022). Enhancement of the Energy Performance of an Existing Building Using a Parametric Approach. *J. Energy Eng*, *149*, 04022057.

[17]. Park, Y. S., & Lek, S. (2016). Artificial neural networks: Multilayer perceptron for ecological modeling. In Developments in environmental modelling (Vol. 28, pp. 123-140). Elsevier.

[18]. Misra, D., Samanta, B., Dutta, S., & Bandopadhyay, S. (2007). Evaluation of artificial neural networks and kriging for the prediction of arsenic in Alaskan bedrock-derived stream sediments using gold concentration data. International Journal of Mining, Reclamation and Environment, 21(4), 282-294.

[19]. Mostafaei, K., & Ramazi, H. (2019). Mineral resource estimation using a combination of drilling and IP-Rs data using statistical and cokriging methods. Bulletin of the mineral research and exploration, 160(160), 177-195.

[20]. Nezamolhosseini, S. A., Mojtahedzadeh, S. H., & Gholamnejad, J. (2017). The application of artificial neural networks to ore reserve estimation at choghart iron ore deposit. روش های تحلیلی و عددی در مهندسی معدن, ٦..(ویژه نامه انگلیسی), ٧٣-٨٣.

[21]. Mostafaei, K., & Ramazi, H. R. (2018). 3D model construction of induced polarization and resistivity data with quantifying uncertainties using geostatistical methods and drilling (case study: Madan Bozorg, Iran. *Journal of Mining and Environment, 9*(4)*, 857–872.

[22]. Mostafaei, Kamran., & Ramazi, H. (2018). Compiling and verifying 3D models of 2D induced polarization and resistivity data by geostatistical methods. *Acta Geophysica*, *66*(5), 959–971.

[23]. Dwarapudi, S., & Rao, S. M. (2007). Prediction of iron ore pellet strength using artificial neural network model. ISIJ international, 47(1), 67-72.

[24]. Abdelhamid, M. M. A., Mousa, B. G., Waqas, H., Elkotb, M. A., Eldin, S. M., Munir, I., ... & Galal, A. M. (2022). Artificial thermal quenching and salt crystallization weathering processes for the assessment of long-term degradation characteristics of some sedimentary rocks, Egypt. Minerals, 12(11), 1393.

[25]. Gouda, M.A. (1996). Trend Analysis and Simulation Modeling of El-Gidida Iron Ore Deposits.

Unpublished Ph.D .Thesis, Mining and Petroleum Engineering Department, AL-Azhar University.

[26]. Badr Hussein, K., Ibrahim, M., & Mousa, B. G. (2023). Modeling and Analysis of Shoreline Change in the Sidi Abdel Rahman Coast Area, Egypt. NAŠE MORE: znanstveni časopis za more i pomorstvo, 70(1), 23-37.

[27]. Mousa, B.G., Embaby, A.K., & Osman, M.E. (2015). GIS Technology for El-Gedida Iron Ore to satisfy the Requirements of Egyptian Blast Furnace. *International Journal of Scientific & Engineering Research*, *6*(9), 8–14.

[28]. El-Araf, M.M., & Lotfy, Z.H. (1989). Genetic Karst Significance of the Iron Ore Deposits of El Baharia Oasis, Western Desert, Egypt . *Reprint from the Annals of the Geological Survey of Egypt*, *15*:1-30.

[29]. Galal, El-Habaak., Mohamed, Askalany., Mohamed, Faraghaly., & Mahmoud, Abdel-Hakeem. (2016). Application of Microscopy Coupled With Image Analysis Technique In Ore Dressing: A Case Study from El-Gedida Iron Mine, El-Bahariya Oasis, Western Desert, Egypt. *International Journal of Basic and Applied Science*, *Vol. 04, No. 03*, pp. 33-41.

[30]. El Aref, M., Abd El-Rahman, Y., Zoheir, B., Surour, A., Helmy, H. M., Abdelnasser, A., & *et al*. (2020). Mineral Resources in Egypt (I). *Metallic Ores*, 521–587.

[31]. El Bassyony, A A. (2005). Bahariya teetotumensis n.gen.n.sp. from the Middle Eocene of Egypt. *Rev. Paléobiol*, *24*, p.319-329.

[32]. Kennedy, K. H. 2009. Introduction to 3D Data. John Wiley & Sons, Inc., Hoboken, New Jersey.

[33]. Mousa, B.G., Embaby, A.E., & Osman, M.E.(2016). Applications of GIS in Operations of Open Cast Mining. *LAP Lambert Academic Publishing*, Germany, ISBN 3659882410.

[34]. Liu, H., & Wu, C. (2019). Developing a Scene-based Triangulated Irregular Network (TIN) Technique for Individual Tree Crown Reconstruction with LiDAR Data. *Forests*, *11*, 28.

[35]. Mousa, B.G., Embaby, A. Kh., and Osman, M.E. (2014). Creating Data Base for Um Salamah-El Sibaiyyah- East Nile Valley Phosphate Ore by using Geographic Information System to Assist in Mining Process Management. *Journal of Al-Azhar University Engineering Sector (JAUES), 9*(1): 1548-1556.

[36]. Sadawy, M. M., & M, A. El ashkar, (2012).Prediction and modeling of corrosion in steel oil storage tank from non-destructive inspection. *Journal of Al Azhar University Engineering Sector*, *7*(4), 42-53.

[37]. Sadawy, M. M., Ismael, A. F., & Goud, M. A. (2015).Geostatistical Analysis for Corrosion in Oil Steel Tank. *American Journal of Science and Technology*, *Vol. 2, No. 2*, pp. 38-42.

[38]. Taany, R.A., Tahboub, B., & G, A. (2009). Saffarini, Geostatistical analysis of spatiotemporal variability of groundwater level fluctuations in Amman-Zarqa basin, Jordan: A case study, *Environ. Geo. l57*, 525-535.

[39]. Mosaad, M. S., & Eltohamy, R. Elsharkawy.(2013). Prediction and Modelling of Corrosion in Steel Storage Tank using Non-destructive Inspection. *Journal of Materials Science and Engineering, B 3 (12).* pp.785-792

[40] Corte, A.F., Calaforra, J.M., Espinos, R. J., & Martos, F.S.(2006). Geostatistical spatiotemporal analysis of air temperature as an aid to delineating thermal stability zones in a potential show cave: Implications for environmental management. *Jour. of Envir. Manag, 81,* 371-383.

[41] Mousa, B.G., Shu, H., Freeshah, M., & Tariq, A. (2020). A Novel Scheme for Merging Active and Passive Satellite Soil Moisture Retrievals Based on Maximizing the Signal to Noise Ratio. *remote sens*ing, 12, 3804.

[42]. Gomah, M.E., Li, G., Khan, N.M., Sun, C., Xu, J., Omar, A.A., Mousa, B.G., Abdelhamid, M.M.A., & Zaki, M.M.(2022). Prediction of Strength Parameters of Thermally Treated Egyptian Granodiorite using Multivariate Statistics and Machine Learning Techniques. *Math*ematics, *Vol. 10*, Page 4523 2022, 10, 4523.

[43]. Mousa, B.G., & Shu, H. (2020). Spatial Evaluation and Assimilation of SMAP, SMOS, and ASCAT Satellite Soil Moisture Products Over Africa Using Statistical Techniques. *Earth Sp. Sci*,7, 1–16.

[44.] Abdelhamid, M.M.A., & Mousa, B.G. (2023). prediction method for abrasion loss rate of some Egyptian carbonate rocks due to cyclic salt crystallization weathering using physico-mechanical deterioration: insights from laboratory investigations. *Acta Geod. Geophys*, 1–18.

[45]. Freeshah, M., Zhang, X., Şentürk, E., Adil, M. A., Mousa, B. G., Tariq, A., ... & Refaat, M. (2021). Analysis of atmospheric and ionospheric variations due to impacts of super typhoon Mangkhut (1822) in the Northwest Pacific Ocean. *Remote Sensing*, *13*(4), 661.

پیش‌بینی عیار سنگ آهن با استفاده از شبکه عصبی مصنوعی، روش محاسباتی و تکنیک‌های زمین‌آماری در منطقه الجزرا، صحرای غربی، مصر

اشرف اف. اسماعیل‌^{۱،۲}، عبدالرحیم امبابی *^۱، فیصل ع.علی^۱، ح.ا. فراق^۱، سید گماع^۱، محمد الواگیه^۳ و بی.جی. موسی^۱

۱ .گروه مهندسی معدن و نفت، دانشکده فنی، دانشگاه الازهر، قاهره، مصر

۲. دانشکده مهندسی و فناوری، دانشگاه آینده در مصر (FUE) ، قاهره، مصر

۳. گروه مهندسی معدن، نفت و متالورژی، دانشکده فنی، دانشگاه قاهره، قاهره، مصر

* نویسنده مسئول مکاتبات: Abdel-raheemkhalifa.12@azhar.edu.eg

چکیده:

فرآیند تخمین منابع معدنی نیاز به پیش‌بینی دقیق عیار بر اسـاس داده‌های محدود حفاری دارد. درجه یک عامل مهم در انتخاب پروژه‌های معدنی مختلف برای سـرمایه گذاری و توسـعه اسـت. هنگامی که الزامات ثابت برآورده نمی‌شـود، روش‌های زمین آماری برای برآورد ذخیره چالش برانگیز اسـت. شـبکه‌های عصـبی مصنوعی (ANN) جایگزین بهتری برای تکنیک‌های زمین‌آماری هستند زیرا زمان پردازش کمتری برای ایجاد و اعمال می‌برند. برای پیش‌بینی عیار سنگ آهن در منطقه الجزرا در واحه البهاریا، صحرای غربی مصر، یک مدل جدید شبکه عصبی مصنوعی (ANN)، روش‌های زمین آماری (واریوگرام ها و کریجینگ معمولی) و شـبکه نامنظم مثلثی (TIN) در این مطالعه به کار گرفته شـدند. مدل‌های زمین آماری و تکنیک TIN توزیع متمایز عناصـر سـنگ آهن را در منطقه مورد مطالعه نشان داد. در ابتدا، توابع سیگموئید قهوه‌ای مایل به زرد و سیگموئید لجستیک در تعداد مختلف نورون برای انتخاب بهترین مدل ANN از یک و دو لایه پنهان با استفاده از تابع خروجی خطی خالص لوونبرگ-مارکوارت مقایسه شدند. مدل ANN ارائه شده سنگ آهن را به عنوان تابعی از عیار کلر، SiO_2، و MnO٪ با ضریب همبستگی ۰.۹۴ تخمین می‌زند. مدل ANN پیشنهادی را می‌توان برای هر مجموعه داده دیگری در محدوده با دقت قابل قبول اعمال کرد.

کلمات کلیدی: شبکه عصبی مصنوعی، عیار سنگ آهن، منطقه الجزره، زمین آمار، GIS.